High-field planar magnetization processes in $Tm_2Fe_{14}B$

1992 J. Phys.: Condens. Matter 4 6629

(http://iopscience.iop.org/0953-8984/4/31/014)

J. Phys.: Condens. Matter 4 (1992) 6629–6638. Printed in the UK

High-field planar magnetization processes in $Tm_2Fe_{14}B$

Hong-Shuo Li and J M Cadogan

School of Physics, The University of New South Wales, Kensington, NSW 2033, Australia

Received 9 March 1992, in final form 8 May 1992

Abstract. Magnetization curves for $Tm_2Fe_{14}B$, at 4.2 and 78 K, have been calculated for external magnetic fields up to 200 T, applied in the a–b plane, by using a first-principles model of the Tm–Fe exchange and crystal-field interactions. It has been shown that at 4.2 K there is a field-induced planar fan-magnetic structure for moderate fields applied along the [100] direction. In this applied field range, the Fe-sublattice magnetization is not parallel to the applied field direction. First-order magnetization processes are predicted at 4.2 K, at critical fields of $\mu_0 H_{cr1}$ = 47.9 T (with a corresponding change in magnetization of ΔM = 6.90 μ_B FU^{-1}) and $\mu_0 H_{cr2}$ = 73.5 T (ΔM = 9.94 μ_B FU^{-1}) for [100] and $\mu_0 H_{cr1}$ = 59.8 T (ΔM = 7.89 μ_B FU^{-1}) for [110], respectively. At 78 K, a ferri→ferromagnetic transition has been identified in both the [100] and [110] magnetization curves. Initially, the Tm moments are canted about the negative Fe-sublattice magnetization direction. When the external applied field increases, the magnitudes of the Tm moments decrease and vanish at the critical field, $\mu_0 H_{fr}$ = 62.2 T, which is exactly equal to the exchange field acting on the Tm^{3+} ions. With further increases in applied field, the magnitudes of the Tm moments, which are now canted along the positive Fe direction, increase again.

1. Introduction

Since the discovery of the ternary $R_2Fe_{14}B$ (R = rare-earths) series, there have been extensive studies of their intrinsic magnetic properties [1–3]. In particular, the exchange and crystal-field interactions have been studied in great detail [4–6]. Amongst these compounds, those with a positive second-order Stevens coefficient α_J i.e. Sm, Er, Tm and Yb, exhibit an easy plane anisotropy at low temperatures [1–3]. It is well established that the $Er_2Fe_{14}B$ and $Tm_2Fe_{14}B$ compounds adopt a spontaneous in-plane canted magnetic structure, and undergo a planar→axial spin reorientation with increasing temperature, due to the competing contributions of the anisotropies of the R and 3d sublattices. The spin reorientation temperatures are 324 K and 313 K for $Er_2Fe_{14}B$ and $Tm_2Fe_{14}B$ respectively [7–12]. The planar canted magnetic structure consists of one Fe-sublattice magnetization lying along [100], and four in-plane R magnetic moments canted around the [$\bar{1}$00] direction, with a ferrimagnetic R–Fe coupling [13, 14]. This type of magnetic structure shows several interesting features, e.g. complex magnetization processes, spin reorientations and spin-flop (*vide infra*), which can be used to determine accurately the exchange and crystal-field interactions acting on the R^{3+} ions. It has been shown that the dominant crystal-field contribution to the planar anisotropy is the second-order orthorhombic (mm point symmetry) term, $B_{22}O_{22}$ [15], which is mainly responsible for the in-plane canted magnetic structures found in $Er_2Fe_{14}B$ and $Tm_2Fe_{14}B$.

0953-8984/92/316629+10$04.50

From some simple theoretical considerations [16–19], a sudden change in the magnetic structure from ferri→ferromagnetic at a critical applied magnetic field is expected for these kinds of ferrimagnetic compounds. A particular case of a ferri→ferromagnetic transition is the so-called *spin-flop* transition in which the magnitude of the magnetic moments remains constant during the transition. Hiroyoshi *et al* [16] and Kido *et al* [17] claimed that some incipient signs of the spin-flop transition are evident in their high-field (up to 40 T and 50 T respectively) magnetization measurements on $Er_2Fe_{14}B$ and $Tm_2Fe_{14}B$. These authors expected to see a spin-flop transition but it was unfortunately not possible as their maximum applied field is just below the critical fields. More recent high-field magnetization measurements on a [100]-oriented powder sample of $Er_2Fe_{14}B$ [20,21] showed a sudden upturn in magnetization, $\Delta M \simeq 4\mu_B/FU^{-1}$ at a field of about 42 T. Generally, one expects a change in magnetization of $\simeq 2M_R$ in the case of a collinear ferrimagnetic to collinear ferromagnetic transition (which for $Er_2Fe_{14}B \simeq 18\ \mu_B\ FU^{-1}$). Radwanski *et al* [5], Yamada *et al* [6] and Zhao and Jin [22] used a simple three-sublattice model with only second-order crystal-field interactions and an Fe-sublattice magnetization rigidly fixed to the [100] direction in their analyses of such magnetic data. These assumptions led to unsatisfactory agreement between experiment and theory. Kohashi *et al* [21] used a classical five-sublattice model with a phenomenological second-order anisotropy term and so were unable to give a full account of such complicated magnetic structures, despite the good qualitative predictions. In particular, these models [5,6,18,20,22] are unable to explain the low value of the experimentally observed ΔM; this can only be explained *qualitatively* by the classical five-sublattice theory [21]. A *quantitative* analysis of this phenomenon can only be achieved within a more sophisticated first-principles theory in terms of exchange and crystal-field interactions [4]. Our previous paper [15] gave a quantitative description of the complicated magnetization processes in $Er_2Fe_{14}B$, at 4.2 K and 78 K. We showed that before the full ferri→ferromagnetic transition occurs there are several field-induced intermediate in-plane fan-magnetic structures.

In this present work, we extend our theoretical work to give a full account of the magnetic behaviour of $Tm_2Fe_{14}B$ for high applied magnetic fields up to 200 T. We will show that two types of high-field magnetization process occur in the theoretical high-field magnetization curves. The origin of the intermediate planar fan-magnetic structures within the ferri→ferromagnetic transition is discussed. We will demonstrate that the interplay of the external magnetic field and the Tm–Fe exchange interaction leads to zero Tm magnetic moments at a critical field, in the presence of the crystal-field interaction of the Tm^{3+} ions.

2. Theoretical background

Table 1 shows a set of crystal-field parameters and the exchange coefficient n_{TmFe} which were deduced for $Tm_2Fe_{14}B$ [13,14] from fits to single-crystal magnetization curves obtained with an external magnetic field up to 18 T. This set of parameters reproduces well (i) the in-plane canted spin structure and (ii) the plane-axis spin reorientation at 313 K, as observed. In the $R_2Fe_{14}B$ structure, the R ions occupy two crystallographically inequivalent sites, 4f and 4g (using the notation of Givord *et al* [23]), both with orthorhombic point symmetry mm. Each crystallographic R site splits into two magnetically inequivalent sites having different signs of the crystal-field

coefficients A_{n2}, A_{n6} (n = 2, 4 and 6). We note that the signs of A_{22} for these four Tm sites are f_1: −; f_2: +; g_1: +; and g_2: −. This difference in sign is due to a rotation by 90° about the c-axis between the orientation of the local symmetry axes of the atoms located in the crystallographic planes $z = 0$ and $z = 1/2$. Hence, the spin structure resulting from this model consists of four R sublattices oriented about a rigid Fe sublattice. A spontaneous canted spin structure was predicted, with this set of parameters, in which the in-plane Tm magnetic moments at the f and g sites cant symmetrically with angles of $\phi_f = 13.4°$ and $\phi_g = 27.1°$, referred to the negative Fe-sublattice magnetization direction ([$\bar{1}$00]), which are in excellent agreement with the experimental results: $\phi_f = 14.9 \pm 1.8°$, $\phi_g = 34.1 \pm 6.4°$ [9].

Table 1. Crystal-field coefficients and the Tm–Fe exchange coefficient used in our calculations [13,14].

	A_{20} (Ka_0^{-2})	A_{22} (Ka_0^{-2})	A_{40} (Ka_0^{-4})	A_{44} (Ka_0^{-4})	A_{60} (Ka_0^{-6})	A_{64} (Ka_0^{-6})	n_{TmFe} (μ_0)
f site	+258.1	±204.5	−12.3	+34.7	−1.75	−26.5	135
g site	+261.8	±617.0	−10.8	−32.5	−1.70	−10.1	135

The first-principles exchange and crystal-field model used for the present work has been described in great detail in [4]. Here, we will summarize briefly the basic equations. The single-ion rare-earth Hamiltonian used in the calculations is

$$H_R = B_{ex} \cdot 2(g_J - 1)J\mu_B + H_{cf} + \mu_0 H \cdot g_J J \mu_B. \tag{1}$$

The first term is the exchange interaction which in general contains two contributions, R–Fe and R–R; as the R–R exchange is usually very small compared to the R–Fe exchange in the rare-earth iron-rich intermetallic compounds [24] (less than 5% of the R–Fe exchange), we neglect it in the present model. The exchange field acting on the Tm^{3+} ions is given by $B_{ex} = -n_{TmFe}\langle M_{Fe}\rangle$. The third term is the Zeeman term which accounts for the effect of an externally applied magnetic field, H. The single-ion crystal-field Hamiltonian of the Tm^{3+} ions is

$$H_{cf} = \sum_n \sum_m B_{nm} O_{nm} \tag{2}$$

where the $\{O_{nm}\}$ are operator equivalents and the $\{B_{nm}\}$ are the crystal-field parameters which are related to the so-called crystal-field coefficients $\{A_{nm}\}$ by

$$B_{nm} = \theta_n \langle r^n \rangle A_{nm} \tag{3}$$

where θ_n are the Stevens factors for the rare-earth ion [25] and $\langle r^n \rangle$ are the nth radial moments averaged over the 4f electronic shell, which have been tabulated by Freeman and Desclaux [26]. There are only nine non-vanishing terms for each R site in equation (2) due to the point symmetry and a detailed description has been given in our previous paper [4]. In the present calculations, the values of the Fe-sublattic magnetization, $\langle M_{Fe}\rangle$, at 4.2 K and 78 K are taken to be 31.7 and 31.4 μ_B FU^{-1} [27], respectively. In this work, we are only looking at the planar magnetization processes which implies that no contribution to the in-plane anisotropy

from the Fe sublattice is expected (e.g. the Fe-sublattice anisotropy energy is constant and equals the Fe-sublattice second-order anisotropy constant K_1^{Fe}). Since the Fe-sublattice magnetization is assumed to be rigid we need not consider the strong Fe–Fe exchange interaction explicitly here. The total energy of the $Tm_2Fe_{14}B$ formula unit can thus be found after diagonalization of the Tm Hamiltonian (equation (1)) and is defined as follows

$$E_{total} = K_1^{Fe} - \mu_0 \boldsymbol{H} \cdot \langle \boldsymbol{M}_{Fe} \rangle + \frac{1}{2} \sum_i F_R(Tm^{(i)}) \tag{4}$$

where the free energy of the Tm^{3+} ions is calculated from the relation $F_R = -k_B T \ln Z_R$ (where Z_R is the partition function of the Tm^{3+} ions), and i runs over the four magnetically inequivalent Tm^{3+} ions: f_1, f_2, g_1 and g_2. The magnetic structure therefore is determined by minimizing E_{total}, by rotating the Fe-sublattice magnetization direction at given applied field and temperature. The resulting magnetic moments (m) of the Tm^{3+} ions are calculated from the obtained eigen-functions, by using the relation $m = (\langle L \rangle + 2\langle S \rangle)\mu_B$.

3. Results and discussion

In figures 1(a) and 2(a), the calculated 4.2 K [100]- and [110]-magnetization curves are plotted. The solid symbols in figure 1(a) represent the experimental data [16]. The agreement between these data and our theoretical results is excellent. It can be seen from these figures that there are two magnetization processes for both curves, namely $\mu_0 H_{cr1} = 47.9$ T and $\mu_0 H_{cr2} = 73.5$ T for [100] and $\mu_0 H_{cr1} = 59.8$ T and $\mu_0 H_s = 147.0$ T for [110]. Both magnetization processes for [100] are first-order (FOMP) with corresponding changes in magnetization of $\Delta M = 6.90\ \mu_B\ FU^{-1}$ and $9.94\ \mu_B\ FU^{-1}$ respectively, while for [110] the first is a FOMP with a corresponding change in magnetization of $\Delta M = 7.89\ \mu_B\ FU^{-1}$ and the second process is the saturation process with an in-plane saturation field, $\mu_0 H_s = 147.0$ T. Table 2 gives the corresponding resulting critical parameters. Figures 1(b) and 2(b) show the in-plane angles (referred to the crystallographic [100] direction), ϕ, of the magnetization of Fe and the four Tm sublattices as a function of the applied magnetic field.

Table 2. Values of the critical fields and the corresponding changes in the magnetization for the magnetization processes at 4.2 K.

	$\mu_0 H_{cr}$ (T)	ΔM ($\mu_B\ FU^{-1}$)	Order
[100]	47.9	6.90	I
	73.5	9.94	I
[110]	59.8	7.89	I
	140.7	—	II

There are three quite distinct regions in the 4.2 K [100]-magnetization curve which correspond to the three types of planar fan-magnetic structure. In the low-field structure (for fields lower than H_{cr1}) both magnetic moments of the f or g group cant symmetrically about the negative direction of the Fe-sublattice magnetization,

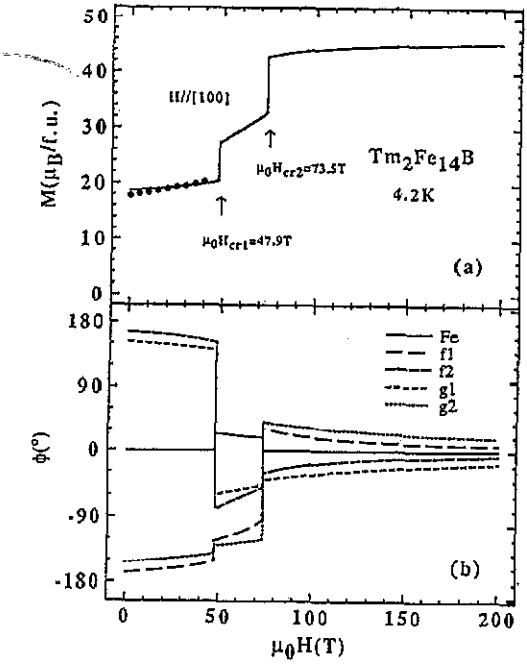

Figure 1. Calculated magnetization curve for an external magnetic field applied along the [100] direction of $Tm_2Fe_{14}B$ at 4.2 K: (*a*) $M(H)$; the solid symbols represent the experimental data of Hiroyoshi *et al* [16] and (*b*) the planar angles of the Fe and Tm moments (referred to the [100] direction).

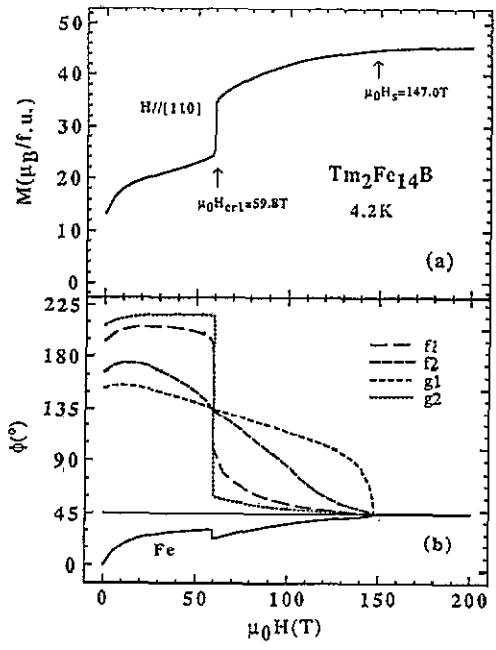

Figure 2. Calculated magnetization curve for an external magnetic field applied along the [110] direction of $Tm_2Fe_{14}B$ at 4.2 K: (*a*) $M(H)$ and (*b*) the planar angles of the Fe and Tm moments (referred to the [100] direction). The solid horizontal line in (*b*) represents the applied magnetic field direction.

which coincides with the applied field direction, [100]. The intermediate structure is *field-induced planar fan-magnetic structure* for applied fields in the range H_{cr1} to H_{cr2}. This structure is characterized by quite unusual spin configurations (see figure 1(*b*)), namely the Fe magnetization cants away from the applied field direction, [100], with a maximum canting angle of 24.9°, while the Tm^{3+} magnetic moments adopt an asymmetric structure. Finally, the high-field structure exists for fields greater than H_{cr2} and up to infinite field and has a similar configuration to the low-field structure except that the Tm–Fe coupling is *canted ferromagnetic* whereas the latter is *canted ferrimagnetic*. The Tm–Fe coupling type may be classified as canted ferrimagnetic when the average coupling angle between the Tm and Fe sublattices is greater than 90° and as canted ferromagnetic coupling when it is less than 90°. Therefore, the field-induced planar fan-magnetic structure is an intermediate structure between the canted ferrimagnetic and the canted ferromagnetic structures.

For the calculated 4.2 K [110]-magnetization curve, there is no clear transition between the canted ferri- and canted ferromagnetic coupling. The Tm^{3+} magnetic moments adopt an asymmetric arrangement about the negative Fe-sublattice magnetization direction for fields lower than the saturation field, $\mu_0 H_s$ = 147.0 T. A collinear

ferromagnetic structure is found for fields greater than the saturation field, H_s, where all the magnetizations of the sublattices are along the applied field direction [110].

Compared to the 4.2 K [100] case, there are three major differences for [110]: (i) the first critical field is larger by about 12 T, (ii) there is only one FOMP in the [110] case compared with two in the [100] case, and (iii) it is possible to saturate the magnetization along the [110] direction ($\mu_0 H_s$ = 147.0 T) whilst for the [100] case it is not ($\mu_0 H_s = \infty$).

As detailed in our previous paper [15], the existence of the field-induced planar fan-magnetic structure derives from the fact that the large decrease in the Zeeman energy of the Tm^{3+} ions upon rotating the Tm moments closer to the applied magnetic field direction, more than compensates for the increase in the Fe-sublattice Zeeman energy, the Tm–Fe exchange energy and the planar anisotropy energy of the Tm^{3+} ions. Thus it is natural to conclude that the planar fan-magnetic structures are truly *field-induced*.

The calculated 78 K [100]- and [110]-magnetization curves are plotted in figures 3(*a*) and 4(*a*), respectively; the solid symbols represent the experimental values reported by Kido *et al* [17]. We see again that the agreement between theory and experiment is very good. There are no FOMPs present in these magnetization curves. However, there is a transition for the [110] case: the Fe-sublattice magnetization is along the applied field direction, [110], and all the Tm moments are along the negative [110] direction at a critical field of, $\mu_0 H_{crl}$ = 18.1 T (see figure 4(*a*)); this is a collinear ferrimagnetic structure.

Figures 3(*b*) and 4(*b*) give the field dependence of the in-plane angles (referred to the [100] direction), ϕ, of all five sublattices' magnetizations. From these figures, we see that there is a sudden change in ϕ for all four Tm moments at a critical field of 62.2 T at 78 K. This change in the orientation of Tm moments does not lead to any change in the total magnetization (see figures 3(*a*) and 4(*a*)); this is only possible if the Tm moments are all zero at the critical field. This is in fact the case as shown in figures 3(*c*) and 4(*c*) where the four individual Tm magnetic moments as a function of applied magnetic field are presented.

From the relative canting angles between the Fe and four Tm sublattices presented in figures 3(*b*) and 4(*b*) we can conclude that the transition, at a field of 62.2 T, marks the change of the coupling scheme from ferri→ferromagnetic. Initially, the Tm moments are canted about the negative Fe-sublattice magnetization direction. When the external applied field increases, the Tm moments decrease and vanish at the ferri→ferromagnetic critical field, $\mu_0 H_{ff}$ = 62.2 T, which is exactly equal to the exchange field acting on the Tm^{3+} ions. For applied fields greater than 62.2 T, the Tm moments increase again but are now canted along the positive Fe direction. The effective field acting on the Tm^{3+} ions is zero when the external applied field exactly equals the exchange field. As a result, the total exchange plus Zeeman splitting of the Tm energy levels vanishes, which leaves only the crystal-field term in equation (1), i.e. $H_R = H_{cf}$. Tm^{3+} is a non-Kramers ion and consequently, in the absence of any effective magnetic field, the pure crystal field splits the ground 4f J-multiplet into a single and six doublets [28]. Thus, $\langle J_z \rangle = 0$ and the Tm^{3+} moment is zero. Since Er^{3+} is a Kramers ion, the pure crystal-field ground states are, at least, a pair of degenerate states leading, in general, to a non-zero $\langle J_z \rangle$ and hence a non-zero Er^{3+} moment in $Er_2Fe_{14}B$ [15].

Unlike in the case of 4.2 K, $Tm_2Fe_{14}B$ shows a clear ferri→ferromagnetic transition at 78 K without any intermediate magnetic structure. The magnitudes of the

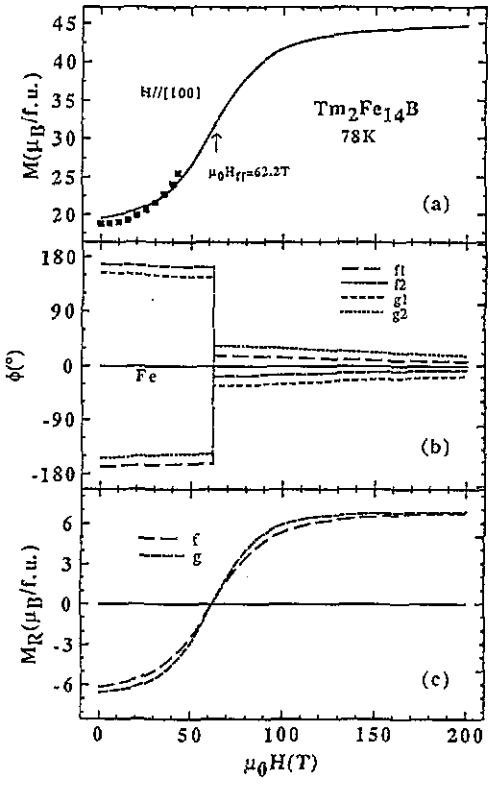

Figure 3. Calculated magnetization curve for an external magnetic field applied along the [100] direction of $Tm_2Fe_{14}B$ at 78 K: (*a*) $M(H)$; the solid symbols represent the experimental data of Kido *et al* [17] and (*b*) the planar angles of the Fe and Tm moments (referred to the [100] direction) and (*c*) the Tm magnetic moments.

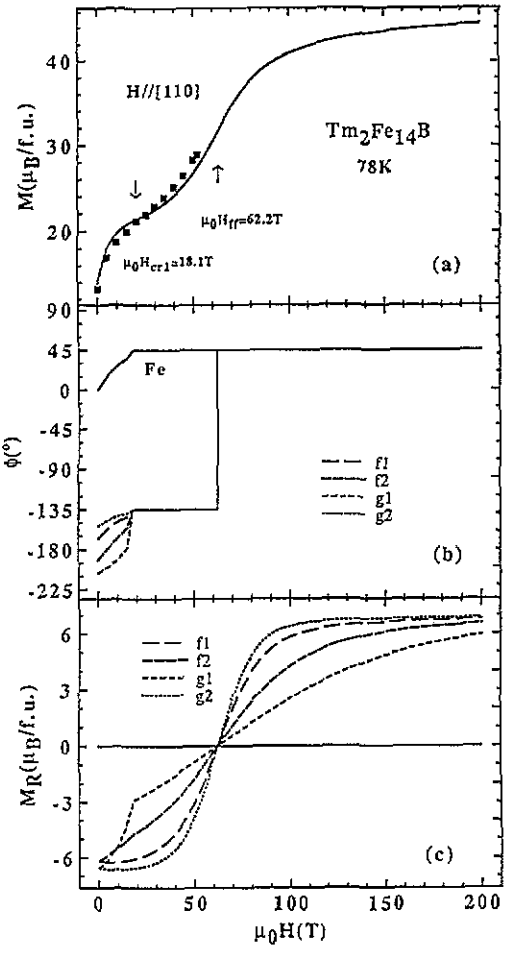

Figure 4. Calculated magnetization curve for an external magnetic field applied along the [110] direction of $Tm_2Fe_{14}B$ at 78 K: (*a*) $M(H)$; the solid symbols represent the experimental data of Kido *et al* [17] and (*b*) the planar angles of the Fe and Tm moments (referred to the [100] direction) and (*c*) the Tm magnetic moments.

Tm moments change continuously throughout the transition, passing through zero moment at the critical field. Hence, this transition is a general ferri→ferromagnetic transition rather than a spin-flop transition.

It is expected that the crystal-field interaction plays a key role in the magnetization processes studied above. First, we consider the planar anisotropy energy of macroscopic Tm^{3+} ions which can be written as [15]

$$E_a(\phi) = \kappa' \sin 2\phi + \kappa'' \cos 4\phi \tag{5}$$

where

$$\kappa' = \tfrac{1}{2}B_{22}\langle O_{20}(0)\rangle$$

$$\kappa'' = \tfrac{1}{16}\left[2B_{44}\langle O_{40}(0)\rangle - B_{64}\langle O_{60}(0)\rangle\right]. \tag{6}$$

Values of κ' and κ'' for the four Tm^{3+} ions in $Tm_2Fe_{14}B$ are listed in table 3. The dominant planar crystal-field term is the second-order orthorhombic term, $B_{22}O_{22}$ (i.e. κ'), and the higher terms (i.e. κ'') give some small modulations superimposed on the $\sin 2\phi$ dependence. There are two minima for ϕ in the range $-180°$ to $+180°$ in the $\sin 2\phi$ dependence: for a positive κ' (for f_2 and g_1) we have $\phi_{min} = 135°$ or $-45°$ while for negative κ' (for f_1 and g_2) we have $\phi_{min} = 45°$ or $-135°$. This creates the possibility that a large change in the Tm moment directions will not cause a large change in the Tm in-plane anisotropy energy. This is the key point for the magnetization processes found in $Tm_2Fe_{14}B$ and $Er_2Fe_{14}B$ [15]; in other words, the crystal-field interactions provide the necessary conditions for having such magnetization processes at 4.2 K.

Table 3. Values of the macroscopic planar anisotropy constant κ' and κ'' at 0 K (in units of K/ion) as defined in equation (3).

	f_1	f_2	g_1	g_2
κ'	−46.38	+46.38	+139.9	−139.9
κ''	− 4.23	−4.23	−4.87	−4.87

The difference in the magnetization curves between 4.2 and 78 K is quite remarkable; in the former there are some FOMPs while in the latter there are only ferri→ferromagnetic transitions. This is mainly due to the relative importance of the crystal-field interaction compared to the exchange and the Zeeman term in these two temperature ranges: at very low temperatures the crystal-field interaction is relatively important and creates a strong planar anisotropy for the Tm^{3+} ions which makes the field-induced planar fan-magnetic structure possible. At 78 K, the crystal field becomes less important and any spin configuration with the Fe sublattice canted away from the applied field direction will be energetically unfavourable; therefore no field-induced planar fan-magnetic structure can occur, and instead the Fe-sublattice magnetization remains along the applied field direction. In this case, as the applied field increases, the effective field (applied field plus exchange field) acting on the Tm^{3+} ions will decrease at first, and pass through zero when the applied field equals the exchange field, then increase in the reverse direction.

Finally, it should be noted that the present calculations give, for the first time, the correct, quantitative planar-magnetization curves, at 4.2 and 78 K, of $Tm_2Fe_{14}B$ for applied fields up to 200 T. All the theoretical predictions in the present calculations are, of course, subject to verification in the future and await further advances in high-magnetic-field technology.

4. Conclusion

In this present work, a full account of the magnetic behaviour of $Tm_2Fe_{14}B$ for high applied magnetic fields up to 200 T, along both [100] and [110], at 4.2 and 78 K, has been given by calculations using a first-principles crystal-field and exchange model. It has been shown that $Tm_2Fe_{14}B$ exhibits several quite distinct magnetic structures depending on the strength of the applied magnetic field. One unusual feature of this magnetic behaviour is that, for applied magnetic fields in a certain range and along the easy magnetization direction, [100], at 4.2 K, the Fe-sublattice magnetization is not parallel to the applied field direction. Ferri→ferromagnetic transitions are predicted for both the [100]- and [110]-magnetization curves at 78 K.

Acknowledgments

This work was supported by the award of a Post-Doctoral Fellowship to HSL from the University of New South Wales. The financial support of the Australian Research Council is gratefully acknowledged.

References

[1] Buschow K H J 1988 *Ferromagnetic Materials* vol 4, ed E P Wohlfarth and K H J Buschow (Amsterdam: North-Holland) ch 1
[2] Herbst J F 1991 *Rev. Mod. Phys.* **63** 819
[3] Buschow K H J 1991 *Rep. Prog. Phys.* **54** 1123
[4] Cadogan J M, Gavigan J P, Givord D and Li H S 1988 *J. Phys. F: Met. Phys.* **18** 779
[5] Radwanski R J and Franse J J M 1989 *J. Magn. Magn. Mater.* **80** 14
[6] Yamada M, Kato H, Yamamoto H and Nakagawa Y 1990 *Phys. Rev.* B **38** 620
[7] Hirosawa S and Sagawa M 1985 *Solid State Commun.* **54** 335
[8] Davis R L, Day R K and Dunlop J B 1985 *Solid State Commun.* **56** 181
[9] Yamada M, Yamaguchi Y, Kato H, Yamamoto H, Nakagawa Y, Hirosawa S and Sagawa M 1985 *Solid State Commun.* **56** 663
[10] Price D C, Day R K and Dunlop J B 1986 *J. Appl. Phys.* **59** 3585
[11] Yelon W B and Herbst J F 1986 *J. Appl. Phys.* **59** 93
[12] Hirosawa S, Matsuura Y, Yamamoto H, Fujimura S, Sagawa M and Yamauchi H 1986 *J. Appl. Phys.* **59** 873
[13] Givord D, Li H S, Cadogan J M, Coey J M D, Gavigan J P, Yamada O, Maruyama H, Sagawa M and Hirosawa S 1988 *J. Appl. Phys.* **63** 3713
[14] Coey J M D, Li H S, Gavigan J P, Cadogan J M and Hu B P 1989 *Concerted European Action on Magnets (CEAM)* ed I V Mitchell, J M D Coey, D Givord, I R Harris and R Hanitsch (London: Elsevier) p 76–97
[15] Li Hong-Shuo and Cadogan J M 1992 *J. Magn. Magn. Mater.* at press
[16] Hiroyoshi H, Saito N, Kido G, Nakagawa Y, Hirosawa S and Sagawa M 1986 *J. Magn. Magn. Mater.* **54–7** 583
[17] Kido G, Kajiwara S, Nakagawa Y, Hirosawa S and Sagawa M 1987 *IEEE Trans. Magn.* **MAG-23** 3107
[18] Radwanski R J, de Boer F R, Franse J J M and Buschow K H J 1989 *Physica* B **159** 311
[19] Cadogan J M 1990 *J. Less-Common Met.* **163** 219
[20] Radwanski R J, de Boer F R, Zhong X P, Yang F M, Li J Y, Kohashi T, Ono M, Date M and Yamagishi A 1991 *J. Magn. Magn. Mater.* **101** 392
[21] Kohashi T, de Boer F R, Radwanski R J, Zhong X P, Yamagishi A and Date M 1991 *J. Phys. Soc. Japan* **60** 3543

[22] Zhao Tiesong and Jin Hanmin 1989 *J. Phys.: Condens. Matter* **1** 8523
[23] Givord D, Li H S and Moreau J M 1984 *Solid State Commun.* **50** 497
[24] Li H S, Li Y P and Coey J M D 1991 *J. Phys.: Condens. Matter* **3** 7277
[25] Stevens K W H 1952 *Proc. Phys. Soc.* A **65** 209
[26] Freeman A J and Desclaux J P 1979 *J. Magn. Magn. Mater.* **12** 11
[27] Tokuhara K, Ohtsu Y, Ono F, Yamada O, Sagawa M and Matsuura Y 1985 *Solid State Commun.* **56** 333
[28] Abragam A and Bleaney B 1970 *Electron Paramagnetic Resonance of Transition Ions* (Oxford: Clarendon) p 713